12 Superconductivity and Magnetism

L. Das, D. Sutter, O. Ivashko, D. Destraz, C. Matt, A. Sidorenko, J. Chang
Associated PhD student - SINERGIA Network: C. Fatuzzo (EPFL)

in collaboration with: Paul Scherrer Institute (M. Dantz, X. Lu, D. E. McNally, N. Plumb, M. Shi, & T. Schmitt), EPFL Lausanne (G. Gatti, N. E. Shaik, H. M. Rønnow & M. Grioni), University of Zurich (C. Monney, A. Schilling & Neupert), University of Central Lancashire, UK (P. G. Freeman), Technical University of Denmark, Denmark (N. B. Christensen), Dipartimento di Fisica 'E. R. Caianiello', Salerno-Italy (V. Granata, R. Fittipaldi & A. Vecchione), Hokkaido University, Japan (T. Kurosawa, M. Oda, & N. Momono), Karlsruher Institut für Technologie, Germany (Konstantin Ilin & Michael Siegel), National Tsing Hua University, Taiwan (T.-R. Chang, H.-T. Jeng), College de France, France (M. Kim & A. Georges), Advanced Light Source, USA (S. Moser, C. Jozwiak, A. Bostwick, E. Rotenberg), Diamond Light Source, UK (T. K. Kim & M. Hoesch)

We present three research projects on strongly correlated electron system studies by complementary techniques such as Resonant Inelastic X-ray Scattering (RIXS), Angle Resolved Photo-Electron Spectroscopy (ARPES) and magnetotransport experiments. Our work covers different electron correlated phenomena. One study provides the electronic structure of the paramagnetic Mott insulating phase of Ca_2RuO_4. Another study is focused on the superconducting fluctuations in the normal state of dirty NbN films. Finally, we have studied the antiferromagnetic spin excitations in the high-temperature superconductor $La_{2-x}Sr_xCuO_4$.

12.1 Nature of the Mott-insulating state of Ca_2RuO_4

A rich variety of electronic instabilities of the Fermi sea emerge as a result of manybody interactions. This leads to fascinating phenomena such as superconductivity, electron- and spin-density wave orders or Mott metal-insulator transitions (MIT). Understanding these different ground states is important in order to gather a full picture of a particular problem. In the case of $Ca_{2-x}Sr_xRuO_4$ ($x = 0, .., 2$), the two end members form diametrically opposed ground states, where Sr_2RuO_4 is a potential chiral $p-$wave superconductor [1] and Ca_2RuO_4 a Mott-insulator [2]. Typically, the Mott-insulating state emerges in systems with a half-filled band and a high ratio of Coulomb interaction U to the bandwidth W. In Ca_2RuO_4, the t_{2g}-manifold is occupied by four electrons, producing a 2/3 filled band, which inhibits a simple explanation of the ground state [3].

Experimentally, it has been found that in the intermediate composition $Ca_{1.5}Sr_{0.5}RuO_4$, metallic transport properties coexist with a Curie-Weiss behaviour of the magnetic susceptibility with $S = 1/2$ per Ru-ion. This may be a possible realisation of a so-called orbital-selective Mott phase (OSMP), where a Mott gap opens for a subset of bands while the others remains metallic [4].

Angle resolved photoemission spectroscopy (ARPES) experiments on $Ca_{1.8}Sr_{0.2}RuO_4$ – the critical composition triggering the MIT – lead to contradicting interpretations of the ground state, favouring [6] or disfavouring [5] the orbital selective Mott scenario.

Extending this idea to Ca_2RuO_4 implies orbital dependent Mott gaps. Another explanation is the crystal field stabilisation of the d_{xy} orbitals due to the c-axis compression of the RuO-octahedra. As a result, the d_{xy} orbitals are completely filled, and thus band insulating while the half-filled d_{yz}/d_{xz} orbitals are Mott localized. Relatively little is known about the low-energy electronic structure of Ca_2RuO_4 and thus impeding a resolution of the effective ground state.

We have conducted ARPES experiments on Ca_2RuO_4 in the paramagnetic Mott-insulating phase at $T = 150\,K$, revealing its band structure. Near the Fermi level, three bands are observed [Fig. 12.1 a), b)]. (*i*) A broadened flat band, extending throughout the whole Brillouin zone ($\mathcal{C}$-band). (*ii*) A fast dispersing band ($\mathcal{B}$-band) evolving around the zone centers and merging with the flat band. (*iii*) Structure in the spectral weight distribution closest to the Fermi level ($\mathcal{A}$-band).

In conjunction with first-principle calculations performed with Density Functional Theory (DFT) including spin-orbit coupling, the observed spectral features can be explained by introducing a phenomenological self-energy $\hat{\Sigma}(\omega)$ in the Green's function $\hat{\mathcal{G}}(\mathbf{k}, \omega) = [\omega - \hat{\mathcal{H}}_{\mathbf{k}} - \hat{\Sigma}(\omega)]^{-1}$ [Fig. 12.1 c)]. In this fashion, we incorporate an enhanced crystal field splitting (Δ_{CF}) of the d_{xy} states and a spectral gap ($\Delta_{xz/yz}$) acting on the d_{yz}/d_{xz} states. Furthermore, we performed Dynamical Mean Field Theory (DMFT) calculations to gain deeper insight [Fig. 12.1 d)]. There the Hund's coupling J and Coulomb interaction U enter as crucial parameters, shaping the spin- and orbital degrees of freedom of the t_{2g}-multiplet. We used $U = 2.3\,eV$ and $J = 0.4\,eV$ which successfully explain correlated phenomena of other ruthen-

ate compounds [7]. The fast dispersing $\mathcal{C}$-band and flat $\mathcal{B}$-band are reproduced and assigned to a d_{xy} and a d_{yz}/d_{xz} orbital character, respectively. Although not smoothly connected to the $\mathcal{C}$-band, the $\mathcal{A}$ close to the Fermi level also carries d_{xy} character. It is found that the d_{xy} orbital driven bands are completely filled and the d_{yz}/d_{xz} bands are Mott-insulating with a band splitting across the Fermi level of order $U + J$. Ca_2RuO_4 is thus a paradigmatic example of a combined band- and Mott-insulator. These results are published in Nature Communications [8].

[1] A. Damascelli *et al.*, Phys. Rev. Lett. **85**, 5194-5197 (2000).

[2] A. V. Puchkov *et al.*, Phys. Rev. Lett. **81**, 2747-2750 (1998).

[3] H. Watanabe *et al.*, PNAS **112**, 14551-14556 (2015).

[4] V. Anisimov *et al.*, Eur. Phys. J. B **25**, 191 (2002).

[5] A. Shimoyamada *et al.*, Phys. Rev. Lett. **102**, 086401 (2009).

[6] M. Neupane *et al.*, Phys. Rev. Lett. **103**, 097001 (2009).

[7] J. Mravlje *et al.*, Phys. Rev. Lett. **106**, 096401 (2011).

[8] D. Sutter *et al.*, Nat. Comm. **8**, 15176 (2017).

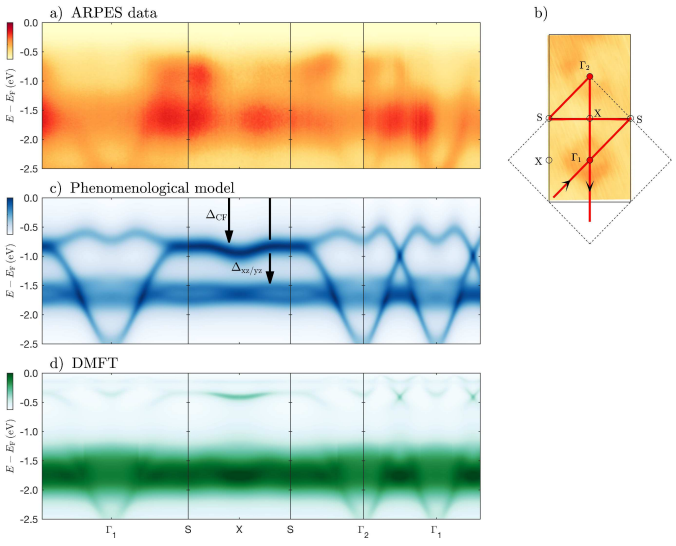

FIG. 12.1 – Band structure of Ca_2RuO_4: (a) ARPES spectra recorded along high symmetry directions with 65 eV circularly polarised light. (b) Constant energy map at binding energy $E - E_F = -2.7$ eV. (c) DFT-derived spectra for Ca_2RuO_4, upon inclusion of a Mott gap $\Delta_{xz/yz} = 1.55$ eV acting on, d_{yz}/d_{xz} bands and an enhanced crystal field $\Delta_{CF} = 0.6$ eV, shifting spectral weight of the d_{xy} bands. (d) DMFT calculation of the spectral function, with Coulomb interaction $U = 2.3$ eV and a Hund's coupling $J = 0.4$ eV.

12.2 Superconducting fluctuations in the Hall effect in a NbN thin film

The transition from a superconductor to a normal conductor above the critical temperature T_c can be caused by a lack of phase coherence, leading to phase fluctuations, or by a destruction of Cooper pairs, leading to (Gaussian) amplitude fluctuations. The nature of the fluctuation is, for example, still debated in the copper-oxide materials (cuprates). The discovery of a pseudogap in NbN has made it an interesting system to compare with the cuprate superconductors [9].

In a recent theoretical paper the Hall effect response of superconducting fluctuations above T_c was calculated for the amplitude fluctuation regime [10]. This theory has already been tested successfully on thin films of TaN [11], which is similar to NbN. However, no pseudogap has been observed in TaN so far. The constraints of the theory are that the electrons must behave three-dimensionally while superconductivity is essentially two-dimensional. This is the case for our film, where the electronic mean free path $\ell = 0.2$ nm is much smaller than the film thickness $d = 11.9$ nm while the coherence length $\xi = 4.3$ nm is comparable.

We have performed Hall effect and resistivity measurements on a thin film of NbN with a critical temperature $T_c = 14.96$ K. The most striking feature of the Hall signal is a sign change from positive in the low-field, fluctuation dominated, region to negative in the high-field, quasiparticle dominated, region. This effect appears in a very small temperature range (≈ 0.5 K) above T_c, and has previously been overlooked [12, 13]. By subtracting the quasiparticle response from the Hall signal, which is linear in the magnetic field strength, we can obtain the pure fluctuation contribution. The same procedure can be applied to the resistivity which then leads to the conductivity tensor of the superconducting fluctuations containing $\Delta\sigma_{xx}$ and $\Delta\sigma_{xy}$. For low temperatures $\Delta\sigma_{xy}$ is linear in field strength and thus the quantity $\nu_H = \Delta\sigma_{xy}/B$ becomes a constant ($\nu_{H,0}$) for $B \to 0$. The quantities $-\Delta\sigma_{xy}$ and $\Delta\sigma_{xx}$ are shown in Fig. 12.2, plotted against $\epsilon = \ln(T/T_c) \approx (T - T_c)/T_c$. The theoretical prediction for the fluctuations in the conductivity is

$$\Delta\sigma_{xx} = \frac{e^2}{16\hbar d}\frac{1}{\epsilon}, \tag{12.1}$$

as calculated by Aslamazov and Larkin [14]. The prediction for the Hall conductivity is a rather complicated expression, but simplifies heavily for the low-field limit, where it becomes

$$\frac{\Delta\sigma_{xy}}{B} = \frac{|e|D\kappa}{3}\frac{e^2}{16\hbar d}\frac{1}{\epsilon^2}. \tag{12.2}$$

Here D is the electron diffusion constant and κ is defined

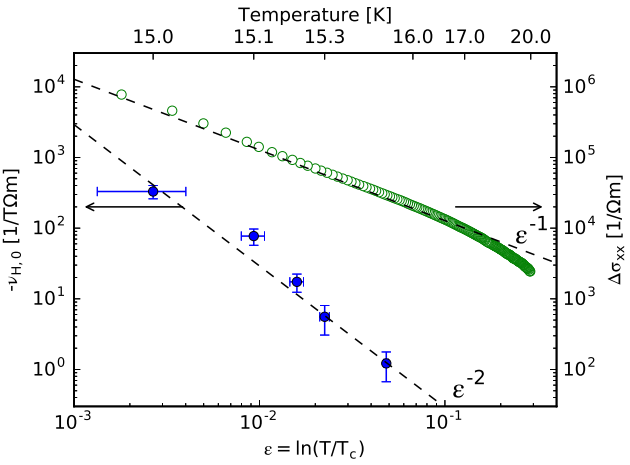

FIG. 12.2 – The low-field value $\nu_{H,0} = \Delta\sigma_{xy}/B$ for $(B \to 0)$ (left axis) and the paraconductivity $\Delta\sigma_{xx}$ (right axis) as a function of ϵ. Dashed lines are the predicted dependencies from Gaussian fluctuation theory without any adjustable parameters. Horizontal error bars correspond to an uncertainty in T_c of 20 mK.

as $-\mathrm{d}\ln(T_c)/\mathrm{d}\mu$, where μ is the chemical potential. The dependence on ϵ and thus temperature is much stronger for $\Delta\sigma_{xy}$ than for $\Delta\sigma_{xx}$. The dashed lines in Fig. 12.2 correspond to these two predictions. As can clearly be seen, the data follow the predicted behaviour perfectly, showing that the superconducting fluctuations in NbN are amplitude fluctuations.

Furthermore, from the value of ν_H, the ghost critical field can be extracted, which we define as the value of the magnetic field, for which ν_H deviates from the linear low-field behaviour. We find that the ghost critical field scales linearly with ϵ. These results are published in Phys. Rev. B [15].

[9] M. Mondal *et al.*, Phys. Rev. Lett. **106**, 047001 (2011).

[10] K. Michaeli *et al.*, Phys. Rev. B **86**, 014515 (2012).

[11] N. Breznay *et al.*, Phys. Rev. B **86**, 014514 (2012).

[12] S. Chockalingam *et al.*, Phys. Rev. B **77**, 214503 (2008).

[13] M. Chand *et al.*, Phys. Rev. B **80**, 134514 (2009).

[14] L. G. Aslamazov and A. Varlamov, Sov. Phys. Solid State **10**, 875 (1968).

[15] D. Destraz *et al.*, Phys. Rev. B **95**, 224501 (2017).

12.3 Damped spin-excitations in a doped cuprate superconductor with orbital hybridization

Considerable research is being undertaken in the quest to reach consensus on the mechanism of high-temperature superconductivity and the associated pseudogap phase in cuprates. The energy scales governing the physical properties of these layered materials therefore remain of great interest. It is known that these materials are characterized by a strong super-exchange interaction $J_1 = 4t^2/U$ where t is the nearest-neighbor hopping integral and U is the Coulomb interaction. To first order, this energy scale sets the band-width of the spin-excitation spectrum. Resonant inelastic x-ray scattering (RIXS) experiments have demonstrated that this band-width stays roughly unchanged across the entire phase diagram [15, 16] of hole doped cuprates. It has also been demonstrated that the cuprates belong to a regime (of t and U) where the second order exchange-interaction $J_2 = 4t^4/U^3$ contributes to a spin-excitation dispersion along the antiferromagnetic zone boundary (AFZB) [17]. Moreover, it is known from band structure calculations and experiments that the next nearest-neighbor (diagonal) hopping integral t' constitutes a non-negligible fraction of t [18]. Empirically [19], the superconducting transition scales with the ratio t'/t whereas Hubbard type models predict the opposite trend [20, 21]. As a resolution, a two-orbital model – in which hybridization of d_{z^2} and $d_{x^2-y^2}$ states suppresses T_c and enhances t' – has been put forward [22].

Here, we address the question as to how t' influences the spin-excitation spectrum at, and in vicinity to, the antiferromagnetic zone boundary. We have therefore studied – using the RIXS technique – slightly underdoped compounds of $La_{2-x}Sr_xCuO_4$ (LSCO) with $x = 0.12$ and 0.145. RIXS spectra (see Fig. 12.3 (a)-(b)) were acquired along high symmetry directions and the resultant pole position of the magnetic excitations were extracted and are presented in Fig. 12.3 (c)-(e). The extracted spin-excitation dispersion of LSCO $x = 0.12$ and 0.145 is to be compared with the magnon dispersion of the parent compound La_2CuO_4 [17, 23]. Along the anti-nodal $(\frac{1}{2}, 0)$-direction comparable dispersions are found. This is consistent with the weak doping dependence reported on LSCO [16] and the $YBa_2Cu_3O_{7-\delta}$ (YBCO) system , [15]. For the nodal $(\frac{1}{4}, \frac{1}{4})$-direction, the dispersion of the doped compound is, however, strongly softened compared to La_2CuO_4 (as also reported for LSCO $x = 0.23$ [24]).

The spin-excitation dispersion of doped LSCO is analyzed using an effective Heisenberg Hamiltonian derived from a $t - t' - t'' - U$ Hubbard model [25]. Within this model the zone boundary dispersion can be quantified by $E_{ZB} = \omega(\frac{1}{2}, 0) - \omega(\frac{1}{4}, \frac{1}{4})$ [26]:

$$\frac{E_{ZB}}{12ZJ_2} \approx 1 + \frac{1}{12}\left[112 - \left(\frac{U}{t}\right)^2\right]\left(\frac{t'}{t}\right)^2. \qquad (12.3)$$

A key prediction is thus that E_{ZB} scales as $(t'/t)^2$ with a pre-factor that depends on $(U/t)^2$.

This effective Heisenberg model is in principle not applicable to doped and hence antiferromagnetically disordered cuprates. However, in the absence of analytical

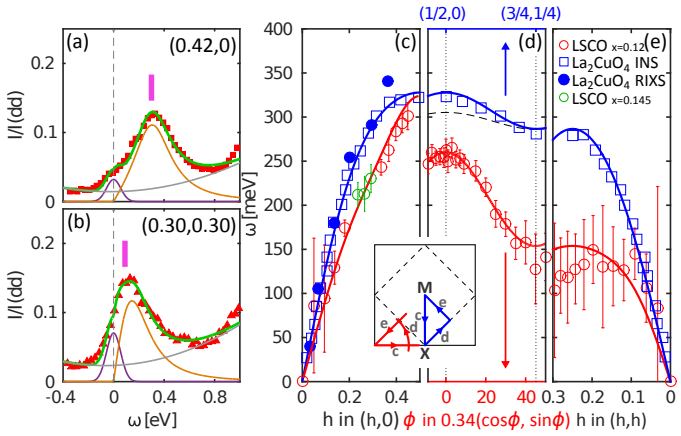

FIG. 12.3 – RIXS spectra for anti-nodal (a) and nodal (b) directions with the indicated in-plane momentum. The fit (solid green curve) is composed of three components: elastic line (purple), spin-excitation (orange) modeled by an anti-symmetric Lorentzian function and a quadratic background (grey). Vertical bars indicate the obtained poles of the Lorentzian function. (c)-(e) dispersion of the magnetic excitations in La_2CuO_4 (blue squares) and $La_{2-x}Sr_xCuO_4$ with $x = 0.12$ (red circles) observed by neutron scattering and RIXS (Ref. [17] and Ref. [23]), and RIXS (this work), respectively. Green circles in (c) are extracted from $La_{2-x}Sr_xCuO_4$ with $x = 0.145$ data. Within the antiferromagnetic zone scheme (indicated by the dashed line in the insert), red and blue cuts c and e are the equivalent anti-nodal and nodal directions. Solid lines in (c)-(e) are fits using a Heisenberg model. In (d) the thin dashed line is the correspective azimuthal scan, for La_2CuO_4, extracted from the above mentioned model.

models, the Heisenberg model serves as a useful effective parametrization tool to describe the damped spin-excitations. Within a single-band tight-binding model, angle resolved photoemission spectroscopy (ARPES) experiments have found that t' decreases slightly with increasing doping [18, 27]. The stronger zone boundary dispersion can thus not be attributed to an increase of t'. Furthermore it is not possible to obtain a good fit to the data using the small value of t' reported in Ref. [18].

This failure combined with the observation of a reduced level splitting between the d_{z^2} and $d_{x^2-y^2}$ states motivates a two-band model. It has been demonstrated that d_{z^2} states contribute to effectively increase the t' hopping parameter [22]. Furthermore, with hybridization of d_{z^2} and $d_{x^2-y^2}$ states, a renormalized Coulomb interaction U is expected. Thus keeping $Z = 1.219$ as in La_2CuO_4 [25] and $t'' = -t'/2$, a satisfactory description (solid line in Fig. 12.3(c)-(d)) of the spin-excitation dispersion is obtained for $t'/t = -0.38$ and $U/t = 6.5$. Notice that a similar ratio of t'/t has previously been inferred from the rounded Fermi surface topology of $Tl_2Ba_2CuO_{6+x}$ [28, 29], a material for which the d_{z^2} states are expected to be much less important [30]. It could thus suggest that $t'/t \approx -0.4$ is common to single layer cuprates but masked in LSCO due to the repulsion between the $d_{x^2-y^2}$ and d_{z^2} bands that pushes the van Hove singularity close to the Fermi level and effectively reshapes the Fermi surface topology [22]. The realistic values of U and Z, suggest that – for LSCO – the two-orbital character of this system is an important ingredient to accurately describe the spin-excitation spectrum.

To conclude, we argue that hybridization between d_{z^2} and $d_{x^2-y^2}$, which is especially strong in LSCO, leads to an enhanced t' and a renormalization of the Coulomb interaction U. Both these effects – consistent with the observations – lead to a stronger zone boundary dispersion within the $t - t' - t'' - U$ Hubbard model.

[15] M. L. Tacon *et al.*, Nat. Phys. **7**, 725 (2011).

[16] M. P. M. Dean *et al.*, Nat. Mater. **12**, 1019 (2013).

[17] N. S. Headings *et al.*, Phys. Rev. Lett. **105**, 247001 (2010).

[18] T. Yoshida *et al.*, Phys. Rev. B **74**, 224510 (2006).

[19] E. Pavarini *et al.*, Phys. Rev. Lett. **87**, 047003 (2001).

[20] S. R. White and D. J. Scalapino, Phys. Rev. B **60**, R753 (1999).

[21] T. Maier *et al.*, Phys. Rev. Lett. 85, **1524** (2000).

[22] H. Sakakibara *et al.*, Phys. Rev. Lett. **105**, 057003 (2010).

[23] L. Braicovich *et al.*, Phys. Rev. Lett. **104**, 077002 (2010).

[24] C. Monney *et al.*, Phys. Rev. B **93**, 075103 (2016).

[25] J.-Y. P. Delannoy *et al.*, Phys. Rev. B **79**, 235130 (2009).

[26] O. Ivashko *et al.*, accepted in Phys. Rev. B, arXiv:1702.02782 (2017).

[27] J. Chang *et al.*, Phys. Rev. B **78**, 205103 (2008).

[28] M. Plate *et al.*, Phys. Rev. Lett. **95**, 077001 (2005).

[29] D. C. Peets *et al.*, New Journal of Physics **9**, 28 (2007).

[30] H. Sakakibara *et al.*, Phys. Rev. B **85**, 064501 (2012).